Transition on Swept Leading Edges at Mach 3.5

T. R. Creel Jr.,* I. E. Beckwith,† and F. J. Chen‡
NASA Langley Research Center, Hampton, Virginia

Data and correlations for transition from laminar to turbulent flow on 45- and 60-deg swept cylinders are presented. The data were obtained at Mach 3.5 in the Pilot Low-Disturbance Wind Tunnel at NASA Langley. Freestream noise levels were varied during the test program from extremely low values that were essentially in the instrument noise range to much higher values approaching those in conventional wind tunnels. The results show that end plates or large trips near the upstream end of the cylinders cause turbulent flow along the entire attachment line of the models over the freestream test Reynolds number range (based on cylinder diameter) of approximately $1.0\times10^5 < R_{\infty,D} < 1.6\times10^6$. When all end disturbance sources are removed, transition occurs on the attachment lines at $R_{\infty,D} \simeq 7\text{–}8\times10^5$ independent of freestream noise levels and in agreement with previous correlations. With the addition of small roughness elements on the cylinder attachment lines, transition occurs at lower values of the Reynolds number, depending on both the roughness height and the wind-tunnel noise level. Limited data obtained off the attachment line indicate that the effects on transition of end disturbances, roughness, and wind-tunnel noise are generally similar to those on the attachment lines.

Nomenclature

D = cylinder diameter
d = diameter of trip wires
k = trip height
ℓ = streamwise length of end plates upstream of cylinder attachment lines
M = Mach number
P = pressure
q = velocity vector
r = recovery factor, $(T_r - T_e)/(T_o - T_e)$
R = unit Reynolds number, $\rho q/\mu$
$R_{\infty,D}$ = Reynolds number based on freestream flow conditions and cylinder diameter, $(\rho q/\mu)_\infty D$
$R_{\theta,s}$ = spanwise momentum thickness Reynolds number at attachment line, $(\rho v/\mu)_s \theta_s$
$R_{\Delta X}$ = freestream Reynolds number based on axial length of quiet test core
$\bar{R}$ = attachment line boundary-layer parameter, $(\rho v/\mu)_s \eta$
s = spanwise distance from model tip
T = absolute temperature
V = velocity component normal to local inviscid streamline
u,v,w = boundary-layer velocity components in x,y,z directions
X,Y,Z = nozzle coordinates, see Fig. 3 (X is the axial distance from the throat)
$\Delta X, \Delta Y, \Delta Z$ = quiet (laminar) test core axial length, height, and width (see Fig. 1)
x,y,z = boundary-layer coordinates; chordwise, spanwise, and normal to model surfacing, respectively
γ = ratio of specific heats
δ = attachment line boundary-layer thickness
η = boundary-layer thickness scale at attachement line, $[\mu/\rho(du_e/dx)]_s^{1/2}$
θ = angular chordwise distance from attachment line
θ_s = spanwise momentum thickness at attachment line, $\int_o^\delta \left[\left(1-\frac{v}{v_e}\right)\frac{\rho v}{\rho_e v_e}\right]_{x=0} dz$
Λ = sweep angle
λ = wavelength of surface oil flow streaks caused by crossflow vortices
μ = dynamic viscosity
ν = kinematic viscosity, μ/ρ
ρ = mass density
χ = local crossflow Reynolds number, $(\rho/\mu)_e V_{\max} \delta$

Subscripts

c = centerline
e = local freestream at edge of boundary layer
N = normal to cylinder
o = isentropic stagnation conditions
r = recovery temperature
s = conditions at edge of boundary layer on attachment line
T = transition
Tip = upstream tip of models
w = wall value
$*$ = parameter evaluated at reference temperature T_*
∞ = freestream conditions upstream of bow shock

Superscripts

$(\tilde{\ })$ = root-mean-square of fluctuating values
$(\bar{\ })$ = mean value

Presented as AIAA Paper 86-1085 at the AIAA/ASME 4th Fluid Mechanics, Plasma Dynamics and Lasers Conference, Atlanta, GA, May 12–14, 1986; received Aug. 31, 1986; revision received Jan. 6, 1987.

*Aerospace Engineer, Viscous Flow Branch, High-Speed Aerodynamics Division. Member AIAA.

†Leader, High Speed Boundary Layer, Stability and Transition Group, Viscous Flow Branch, High-Speed Aerodynamics Division. Associate Fellow AIAA.

‡Research Associate, High Technology Corporation, Hampton, VA. Member AIAA.

Introduction

THE development and application of laminar flow control (LFC) techniques to subsonic swept wings has required a detailed understanding of the effects of surface roughness, spanwise contamination, and crossflow vortices on boundary-layer stability and transition in the leading-edge regions.[1-5] Interest in supersonic LFC is increasing because of the possible large gains in performance and range. However, the experimental data base required for supersonic LFC may be adversely affected by the high freestream noise levels present in conventional supersonic wind tunnels. It has been known for many years that this wind-tunnel noise has large adverse effects on boundary-layer stability and transition processes on simple test models such as flat plates and cones (see Ref. 6). With the development and successful operation at NASA Langley of the Mach 3.5 Pilot Low-Disturbance Wind Tunnel,[6] it became possible to determine if transition on swept leading edges is as sensitive to wind-tunnel noise as transition is on simpler models.

Two mechanisms that cause transition in leading-edge regions of swept wings at subsonic speeds are "spanwise contamination" and "crossflow instability." The problem of spanwise turbulent contamination along the attachment line of swept wings was recognized and solved in the early 1960's before laminar flow could be achieved at relatively high Reynolds numbers on swept wings in both the X-21[1,2] and the British Handley Page[3] LFC programs. Wind-tunnel tests were conducted during these programs to develop a better understanding and suitable solutions of the problem. Critical values of the attachment line momentum thickness Reynolds number $R_{\theta,s}$ were found to be about 100 in the presence of large upstream disturbances and about 240 with all disturbances removed. These higher values of $R_{\theta,s}$ were obtained in the X-21 program[2] by the use of strong local suction, leading-edge suction fences, or "backward sweep" of the wing panels from a wing apex stagnation point with an undisturbed laminar boundary layer. In the British program,[3] a protruding, faired bump attached to the leading edge was used to prevent the spanwise propagation of turbulence.

A second mechanism that causes transition near the leading edge of swept wings is crossflow instability.[2] The effects of this mechanism were first observed in flight experiments by Gray[4] as regularly spaced streaks caused by variations in mass transfer from surface coatings. The streaks were aligned in the local streamwise direction and were present over the upstream regions preceding transition on swept-back wings. Later work[7] confirmed that these streaks were caused by corotating vortices resulting from the inflectional instability of the crossflow boundary-layer profiles in the upstream regions of swept wings.

More recently, Poll[5,8-10] has extended and clarified the early work at subsonic speeds on these swept-wing transition mechanisms. In particular, Poll studied the response of the attachment line boundary layer to trip wires of different diameteres d fixed to the surface normal to the wing leading edge. He showed that transition behavior on the attachment line is quite complex and may be separated into four distinct regimes in terms of $R_{\theta,s}$ and d/θ_s. Poll's studies on the crossflow instability mechanism[8-10] showed that in the absence of disturbances on the attachment line, transition farther downstream depended on two parameters, the crossflow Reynolds number χ and $R_{\theta,s}$, rather than on χ alone as was previously thought from earlier studies.[11]

Poll extended his attachment line transition correlations to supersonic speeds[12] with a local boundary-layer parameter $\bar{R}_*$ evaluated at a reference temperature. Poll limited this application to conditions for large trip wires and end disturbances. However, Bushnell and Huffman[13] had shown previously from correlations of a large amount of data for Mach numbers up to 10 and sweep angles of 10–80 deg that when no end disturbances were present, the attachment line flow was always laminar up to values of $R_{\infty,D} \simeq 8 \times 10^5$, which was the upper limit for data available at that time. When large end disturbances were present, transition was generally observed for $R_{\infty,D} \simeq 2 \times 10^5$.

During the present study, transition data were obtained for circular cylinders at sweep angles of 45 and 60 deg in the Mach 3.5 Pilot Low-Disturbance Tunnel[6] over the unit Reynolds number range of 1.0×10^5 to 1.7×10^6 per inch. To investigate the effects of wind-tunnel noise, the models were exposed to both extremely low noise levels (essentially within the instrument noise range) and to much higher levels in the range of conventional supersonic tunnels by moving the

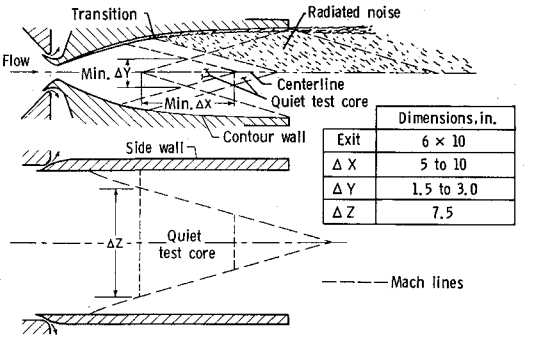

Fig. 1 Quiet test core size and shape in $M_\infty = 3.5$ Pilot Low Disturbance Tunnel.

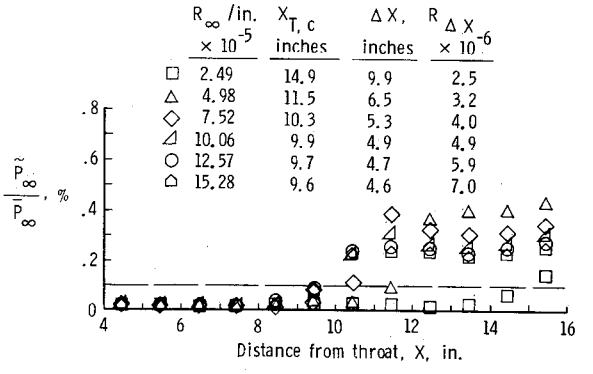

a) Bleed valve open.

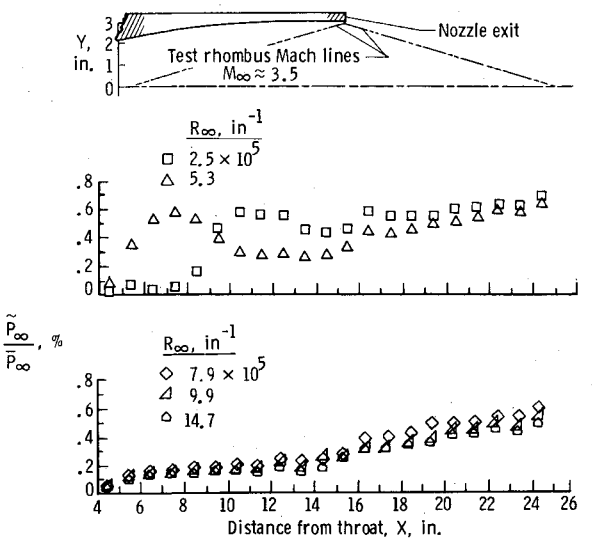

b) Bleed valve closed.

Fig. 2 Normalized rms pressure fluctuations from hot-wire data on the centerline in the Mach 3.5 pilot nozzle.

models downstream and closing a boundary-layer removal valve. Detailed data were obtained along the attachment lines with and without boundary-layer trips and end disturbances. Some limited data off the attachment line from approximately 30–50 deg around the cylinders are also presented.

Apparatus

Facility

Figure 1 shows side and plan views of the Mach 3.5 pilot nozzle.[6] The shape and typical sizes of the quiet flow region are given. Also illustrated are the boundary-layer removal slots upstream of the throat and a typical location of transition on the contour wall with the "bleed" valve open. This bleed valve is used to control the boundary-layer removal flow and, for the present tests, the valve was either fully open or closed. The onset of the radiated noise from the supersonic turbulent boundary-layer eddies occurs at the transition location. The Mach lines extending from this location are the downstream boundaries of the quiet test region, since acoustic disturbances are propagated along Mach lines in supersonic flow. With the bleed valve open, transition on the nozzle wall moves upstream with increasing unit Reynolds number. Therefore, the quiet test core length ΔX decreases with increasing R_∞. The corresponding minimum values of ΔX and ΔY are shown in the figure. The minimum value of ΔZ illustrated on the plan view in the figure is determined by the nozzle width and Mach lines extended downstream from the sidewall acoustic origin region where $M_e \gtrsim 2.5$. The noise radiation from the turbulent sidewall boundary layers then increases significantly.[6]

Figure 2 shows the variation along the nozzle centerline of rms static pressure fluctuations normalized by the mean static pressure $(\tilde{P}/\bar{P})_\infty$ obtained from constant current hot-wire anemometer data. In Fig. 2a, values of ΔX are listed for the test range of R_∞ with the bleed valve open, which results in laminar wall boundary layers and low noise levels of about 0.05% in the upstream part of the test region. The noise levels downstream of the quiet test core increase to values of about 0.25–0.4%. Here, ΔX is defined in inches as $(X_{T,c}-5)$ where $X_{T,c}$ is the location on the centerline where faired curves for the $\tilde{P}/\bar{P}$ data increase above 0.1% and $X=5$ in. is the upstream tip of the Mach 3.5 uniform flow test rhombus.[6]

Figure 2b shows the same type of noise data[6] for about the same range of R_∞, but with the bleed valve closed, which results in turbulent nozzle-wall boundary layers at all but the lowest unit Reynolds number. The noise varies from about 0.15–0.6% throughout the test rhombus, except for $X<8$ in. at the lowest unit Reynolds number. Hot-wire spectral data[6] showed that, when $(\tilde{P}/\bar{P})_\infty \gtrsim 0.1\%$, acoustic energy was always present at high frequencies. This energy peaked at 20–60 kHz, depending on the X station and the bleed valve setting.

Models and Test Locations

The models consisted of 0.030 in. thick stainless steel cylindrical shells of 0.5 and 1 in. outside diameters with both ends sealed and cut off parallel with the freestream flow direction. Stings attached at the midspan location supported the models. Sharp leading-edge end plates could be attached to the upstream end of the models. These end plates were aligned parallel with the freestream flow with their leading edges perpendicular to and upstream of the attachment lines by either 0.25 or 2 in. Chromel-alumel thermocouple wires of 0.01 in. diameter were spot welded to the inside surface of the shells at 0.25 in. intervals along the entire length of the attachment lines. Five additional thermocouples were attached in the same way to each of the 1 in. diameter models at various locations downstream of the attachment line at about midspan. The surfaces of the models were maintained clean and polished to a finish of less than 10 rms μin.

Figure 3 illustrates the upstream and downstream test positions of the models with respect to the quiet test core. In the upstream "quiet" test position and with the bleed valve open, the forward tips of the models were located 5.8 in. downstream from the nozzle throat (except for one test where $X_{\text{Tip}}=4.3$ in.) such that for $R_\infty \simeq 3\times10^5$, approximately 85 and 70% of the attachment line spans on the $\Lambda=45$ and 60 deg models, respectively, were exposed to the extremely low noise levels (see Fig. 2a). As the unit Reynolds number is increased, transition moves upstream on the nozzle contour walls and the corresponding location of increasing noise measured along the centerline also moves upstream. Thus, at $R_\infty \simeq 8\times10^5$/in., $X_{T,c}\simeq 10$ in. (Fig. 2a), then the percentage of the attachment line spans exposed to the low noise levels are reduced to about 75 and 40% for the $\Lambda=45$ and 60 deg models, respectively. In the downstream "noisy" test position and with the bleed valve closed, the forward tips were located at $X=9.8$ in. (illustrated only in the upper part of Fig. 3 by the projected upstream end view) and the full lengths of both models were then exposed to the higher noise levels of about 0.2-0.5% (see Fig. 2b).

Test Procedures and Data Reduction

After the models were mounted in the desired test position, the tunnel flow was started and the stagnation pressure was increased to the first test value, which was generally the lowest value for a given set of conditions. The stagnation pressure and temperature were then held constant while computer plots of the local recovery factors against s were displayed in nearly real time. After these values of r no longer changed with time, the data were recorded and used in the final plots. This process was then repeated at the next higher stagnation pressure until all required data for the desired set of tunnel conditions were completed.

The equation used to calculate the local values of r from the measured skin temperatures and the measured stagnation temperatures combined with the local calculated static temperatures are as follows:

$$r=\frac{T_r-T_e}{T_o-T_e} \tag{1}$$

where on the attachment line

$$\frac{T_e}{T_o}=\frac{T_s}{T_o}=\frac{1+[(\gamma-1)/2]M_\infty^2\cos^2\Lambda}{1+[(\gamma-1)/2]M_\infty^2} \tag{2}$$

At chordwise distances θ form the attachment line, P_e/P_s is assumed to be independent of $M_{N,\infty}$ and Λ; therefore, this

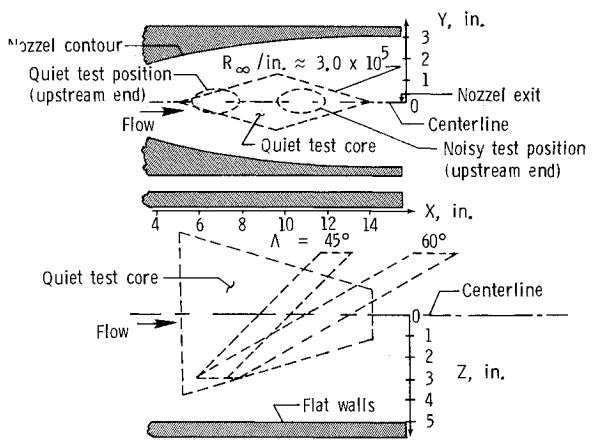

Fig. 3 Test positions of 1-in.-diam models in $M_\infty=3.5$ pilot nozzle.

pressure ratio depends only on θ (see Fig. 3, Ref. 14). Hence,

$$\frac{T_e}{T_o}=\frac{T_e}{T_s}\frac{T_s}{T_o} \tag{3}$$

where

$$\frac{T_e}{T_s}=\left(1+\frac{\gamma-1}{2}M_{N,e}^2\right)^{-1} \tag{4a}$$

and

$$M_{N,e}=\sqrt{\frac{2}{\gamma-1}\left[\left(\frac{P_e}{P_s}\right)^{-(\gamma-1)/\gamma}-1\right]} \tag{4b}$$

Although these equations are derived for infinitely long cylinders, the recovery factor data presented in the next section indicate that reasonable approximations are obtained for the present test cylinders when $s/D>5$.

Results and Discussion

Oil Flow Studies

Visualizations of boundary-layer surface flow effects were obtained from oil flow studies. The mixture used for this purpose was two parts by volume of 350 cs silicone oil to one part titanium powder. A 0.25 in. wide strip of the mixture was applied to the model as a thin coat centered along the attachment line. The tunnel flow parameters were then held constant for approximately 5 min, which was sufficient to stablize the oil flow pattern over the forward part of the model.

Typical photographs of these patterns are shown in Fig. 4. Figure 4a is a side view of the upstream part of the model. A small trip (identified in the figure) of height $k\simeq 0.004$ in. was fixed to the attachment line 6 in. from the upstream tip of the model. The freestream flow direction, with respect to the attachment line (upper edge of model), is indicated by the arrow in the figures. Evidence of crossflow vortices can be seen in Fig. 4a as the series of widely spaced streaks (two typical streaks are labeled "vortices" in the photograph). For this run, typical wavelengths of the vortices, taken as the normal distance between centers of the oil flow streaks, increased from $\lambda\simeq 0.03$ to 0.04 in. as the angular distance from the attachment line is increased from $\theta\simeq 70$ to 90 deg. The ratio of these values of λ to the attachment line boundary-layer thickness[15] is $\lambda/\delta_s\simeq 5$–7 for this Reynolds number of $R_{\infty,D}\simeq 4.6\times 10^5$.

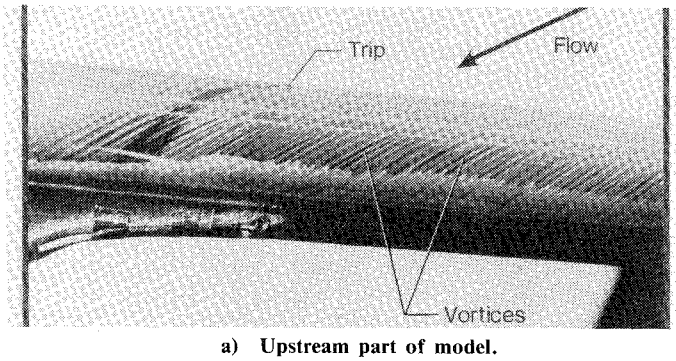

a) Upstream part of model.

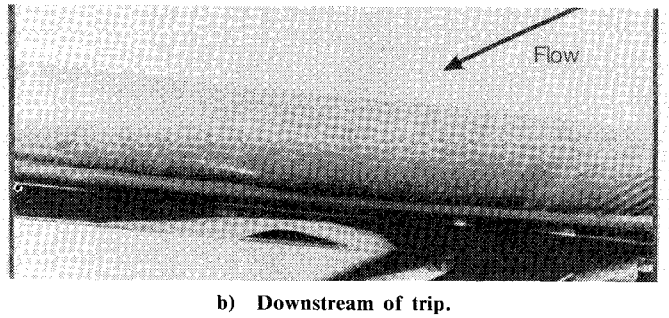

b) Downstream of trip.

Fig. 4 Oil flow patterns with trip ($k\simeq 0.004$ in.) at $s=6$ in. $\Lambda=60$ deg, $D=1$ in., $R_{\infty,D}\simeq 4.6\times 10^5$, bleed valve open, $X_{Tip}=5.8$ in.

Values of λ calculated[§] for the most amplified stationary vortices using compressible linear stability theory are in excellent agreement with the measured values. Downstream of the trip (far left side of Fig. 4a), the wide streak pattern is not evident, presumably because the trip caused turbulent boundary-layer flow. Figure 4b shows more of the downstream part of this model for the same run and, clearly, the wide streaks have been completely obliterated downstream of the trip. The recovery factor data presented in the next section show that this trip did indeed cause transitional or turbulent flow at this value of $R_{\infty,D}$.

Transition from Recovery Factor Variations with s and $R_{\infty,D}$

In this section, the effects of end plates and a large trip near the upstream end of the models on the levels and variations of r with s will be considered first. Cross plots of r against $R_{\infty,D}$ at selected values of s will then be used to evaluate transition Reynolds numbers. Next the effects of wind-tunnel noise and of small trips on transition along the attachment lines for $\Lambda=45$ and 60 deg will be considered. Finally, some data illustrating the effects of tunnel noise and trips on transition downstream of the attachment lines will be shown.

Before these data are presented, it is useful to review the transition correlation parameters to be used herein and their range of values from previous investigations. Relations between the freestream Reynolds number $R_{\infty,D}$ and the local Reynolds numbers $\bar{R}_*$ and $R_{\theta,s}$ are as follows.

The local momentum thickness Reynolds number from Poll[5] is

$$R_{\theta,s}=\left\{\frac{\frac{\nu_\infty}{\nu_s}\sin\Lambda}{1+r\left(\frac{T_o}{T_s}-1\right)}\frac{0.407-0.052\ell n\frac{T_o}{T_s}}{\left[\frac{\nu_\infty}{\nu_w}\cos\Lambda\left(\frac{du_e}{dx}\frac{D}{u_{N,\infty}}\right)_{x=0}\right]^{1/2}}\right\}\times\sqrt{R_{\infty,D}} \tag{5}$$

The local reference length Reynolds number, also from Poll,[12] is

$$\bar{R}_*=\left\{\sqrt{\frac{\nu_\infty}{\nu_*}}\frac{\sin\Lambda}{\left[\cos\Lambda\left(\frac{du_e}{dx}\frac{D}{u_{N,\infty}}\right)_{x=0}\right]^{1/2}}\right\}\sqrt{R_{\infty,D}} \tag{6}$$

where the reference temperature is

$$\frac{T_*}{T_s}=1+0.7\left(\frac{T_r}{T_s}-1\right),\ \text{for } T_w=T_r \tag{7}$$

The ratios of $R_{\theta,s}/\bar{R}_*$ and the quantities within the large braces are listed in Table 1 for both subsonic flow and the present test conditions. Comparisons of these tabulated values show that the ratio and magnitude of the local Reynolds numbers depend on the sweep angle and local Mach numbers behind the bow shock. For comparison with the present results, previous values of these various transition correlation parameters along with their appropriate disturbance and mean flow conditions are given in Table 2.

[§]Private communication from M. R. Malik, High Technology Corporation, Hampton, VA.

Table 1 Values of attachment line parameters

M_∞	Λ, deg	$M_{e,s}$[a]	$R_{\theta,s}/\bar{R}_*$	$R_{\theta,s}/\sqrt{R_{\infty,D}}$	$\bar{R}_*/\sqrt{R_{\infty,D}}$
~0.01 to 0.05	to 80	—	0.404	—	—
3.5	45	1.66	0.479	0.355	0.740
3.5	60	2.39	0.566	0.455	0.804

[a] $M_{e,s}$ is the spanwise Mach number.

Table 2 Values of attachment line parameters at transition

Large upstream disturbance (end plates, roughness, etc.) Parameter	Ref.	No disturbance (no end plates, smooth model, etc.) Parameter	Ref.
$R_{\infty,D} \simeq 2\times10^5$	13	$R_{\infty,D} > 8\times10^5$	13
M_∞ to 8, Λ to 78 deg	13	M_∞ to 9.8, Λ to 82 deg	13
$R_{\theta,s} \simeq 100$–120	5	$R_{\theta,s} \simeq 280$–320	5
$M_{e,s}$ to 1.5	5	Low-speed flow	5
$\bar{R}_* \simeq 250$	12	$\bar{R} \simeq 650$–750	9
$M_{e,s}$ to 6	12	Low-speed flow	9

Applications to new data at $M_\infty = 3.5$

Λ, deg	$R_{\infty,D}\times10^{-5}$ for $R_{\theta,s}$ criteria	$R_{\infty,D}\times10^{-5}$ for $\bar{R}_*$ criteria	Λ, deg	$R_{\infty,D}\times10^{-5}$ for $R_{\theta,s}$ criteria	$R_{\infty,D}\times10^{-5}$ for $\bar{R}_*$ criteria
45	0.8–1.1	1.1	45	6.2–8.1	7.7–10.3
60	0.5–0.7	1.0	60	3.4–5.0	6.5–9.3

Effects of Large End Disturbances

Plots of r against s (not shown herein) for $\Lambda = 45$ and 60 deg with $D = 1$ in. indicated that the levels and trends of r with s were generally different for $s/D < 4$, depending on whether the long or short end plates or a large trip wire ($d = 0.01$ in.) at $s = 0.5$ in. were used. However, for $s/D > 5$, all these conditions resulted in essentially the same constant levels of $r \simeq 0.87$ over the entire test Reynolds number range of $2\times10^5 < R_{\infty,D} < 1.7\times10^6$.

When the models were tested with no end plates (as illustrated in the sketches of Fig. 3) or no trips, the values of r were again approximately constant for $s/D > 5$ at any given value of $R_{\infty,D}$. However, for $R_{\infty,D} \leq 9.1\times10^5$, the levels of r were approximately 0.85, in good agreement with theoretical laminar attachment line values.[16] For $R_{\infty,D} \geq 1.2\times10^6$, the recovery factor values for $s/D > 5$ were again constant but larger at $r \simeq 0.87$, similar to those values previously noted with upstream disturbances present. From these results we conclude that quasi-infinite swept cylinder values were obtained for $s/D > 5$.

The explanation for the two different levels in r of about 0.85 and 0.87 is apparent from Fig. 5, where r is plotted against $R_{\infty,D}$ for $\Lambda = 60$ deg and selected values of $s/D \geq 5$. Figure 5a shows the results for the short end plate and a trip wire with $d = 0.01$ in. located on the attachment line at $s = 0.5$ in. Note the changes in r with $R_{\infty,D}$ are fairly small. (The lower levels of r for the $D = 0.5$ in. model are caused by the relatively larger heat conduction effects in this model, which has the same shell thickness of 0.03 in. as the 1 in. diameter model.) Figure 5b presents data from several runs for both diameter models with no trip or end plate. The increase in r starting at $R_{\infty,D} \simeq 7$–8×10^5 is caused by the onset of transition from laminar to turbulent flow at the attachment line. This value of transition Reynolds number is compared on the figure with previous values from Table 2.

Agreement between these present transition results and the previous criteria is generally good. It is also concluded from Fig. 5 that for the 1 in. diameter model, the laminar attachment line values of r are about 0.84–0.85 and turbulent values are about 0.865–0.875.

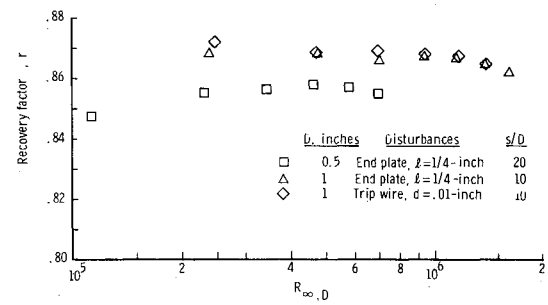

a) End plate or trip wire near upstream end.

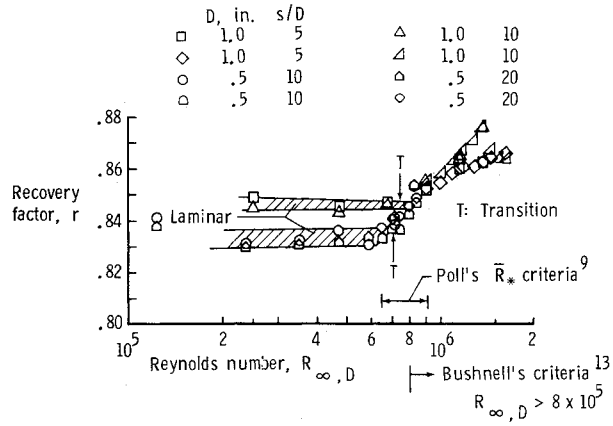

b) No end plates or trips.

Fig. 5 Effects of end disturbances on r variations with $R_{\infty,D}$ on the attachment line. $\Lambda = 6$ deg, bleed valve open, $X_{Tip} = 5.8$ in.

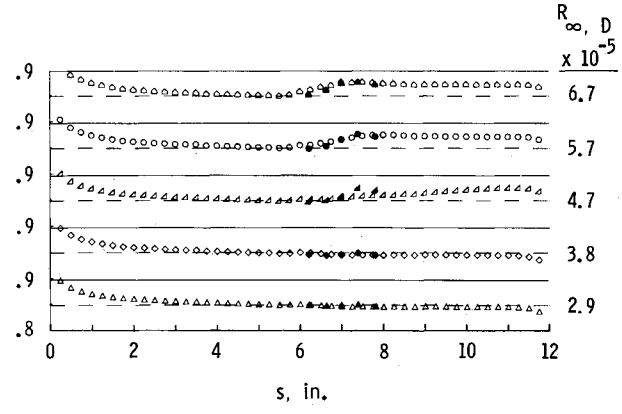

a) Low noise: bleed valve open, $X_{Tip} = 5.8$ in.

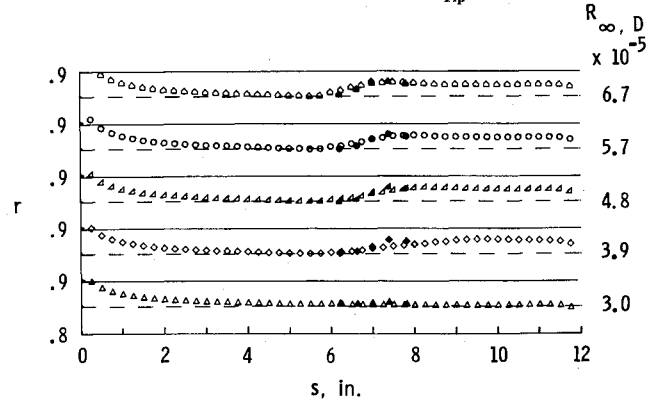

b) High noise: bleed valve closed, $X_{Tip} = 9.8$ in.

Fig. 6 Effects of trip and freestream noise on variations of r with s. $\Lambda = 60$ deg, $D = 1$ in., no end plates. Trip with $k \simeq 0.004$ in. on the attachment line at $s = 6$ in.

Table 3 Values of s and θ

s, in.	θ, deg
7.81	32.1
7.39	39.8
6.99	50.4
6.63	50.4
6.21	50.4

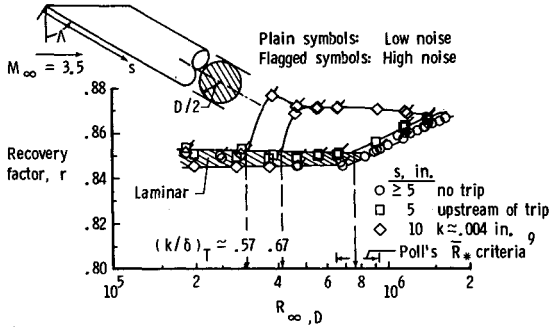

Fig. 7 Effects of freestream noise and a trip on transition at the attachment line for $\Lambda=60$ deg and $D=1$ in. Trip with $k=0.004$ in. located on attachment line at $s=6$ in.

Figure 6 shows typical effects of wind-tunnel noise and a trip on the variation of r with s for the $\Lambda=60$ deg, $D=1$ in. model with no end plates. Note the staggered scales for r. The dashed lines represent the theoretical laminar attachment line value of $r\simeq0.85$.[16] The solid lines represent the usual flat-plate value for turbulent boundary layers of $r\simeq0.89$. The open symbols are from temperature data along the attachment line. The solid symbols plotted at $s\simeq6.2$-7.8 in. are from thermocouples spaced around the cylinder at $\theta\simeq32$-50 deg. In this section, the discussion will be limited primarily to the attachment line values. The trip was made from a small piece of shim stock approximately 0.015×0.030 in. that was bonded to the attachment line at $s=6$ in. The measured height of the installed trip was $k\simeq0.004$ in. Figure 6a shows results for the low tunnel noise condition, that is, with the bleed valve open and $X_{\text{Tip}}=5.8$ in. (see Figs. 2a and 3). Figure 6b is for the high noise condition with the bleed valve closed and $X_{\text{Tip}}=9.8$ in. Upstream of the trip ($s<6$ in.), the levels and trends of r are practically identical over the entire range of $R_{\infty,D}$ for both the low and high noise conditions. Downstream of the trip ($s>6$ in.), the levels and trends in r are again nearly the same except at $R_{\infty,D}\simeq3.9\times10^5$ and 4.8×10^5, where the values of r are generally larger for the high noise case. The trip has apparently caused turbulent boundary-layer flow at lower values of $R_{\infty,D}$ with high tunnel noise than with the low noise. The data off the attachment line respond to the trip and tunnel noise by amounts that are similar to those of the attachment line data.

The attachment line results are summarized in Fig. 7, where r is plotted against $R_{\infty,D}$ for selected values of s from several runs, including those of Fig. 6. The results for no trip (circle symbols) and also upstream of the trip (square symbols) again show transition onset at $R_{\infty,D}\simeq7.5\times10^5$ for both low and high noise (flagged symbols), in agreement with the low noise data of Fig. 5b and previous values from Table 2. However, downstream of the trip at $s=10$ in., transition occurs at lower values of $R_{\infty,D}\simeq3$ or 4×10^5, depending on the tunnel noise. Clearly, the tunnel noise appears to enhance the effect of the trip, but has no effect when there is no trip. (The values of δ used in Figs. 7 and 8 were obtained from Ref. 15.)

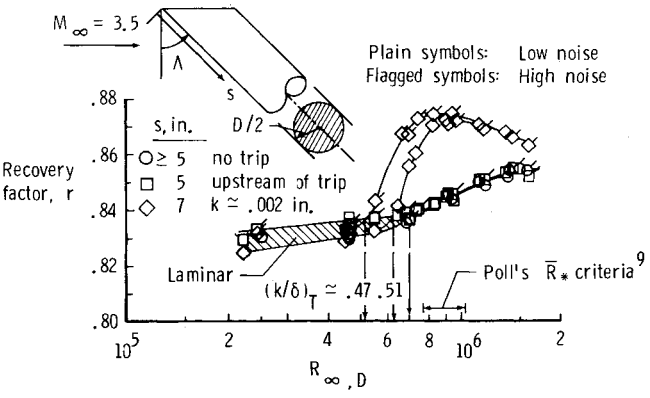

Fig. 8 Effects of freestream noise and trip on transition at the attachment line for $\Lambda=45$ deg and $D=1$ in. Trip with $k=0.002$ in. located on the attachment line at $s=5.5$ in.

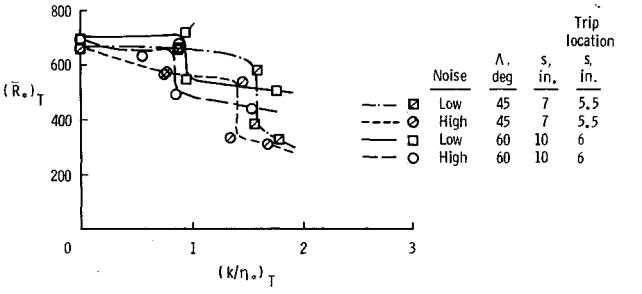

Fig. 9 Effects of normalized roughness heights on transition Reynolds number in terms of reference temperature parameters. The flagged data point for $\Lambda=60$ deg was obtained with $X_{\text{Tip}}=4.3$ in. to get low noise at the trip location.

Plots of r against s for the $\Lambda=45$ deg, $D=1$ in. model for several runs with different trips located on the attachment line at $s=5.5$ in. also indicated that transition occurred downstream of the trips at lower values of $R_{\infty,D}$ with high noise than with low noise. The values of transition Reynolds numbers were again determined from cross plots of r against $R_{\infty,D}$ at selected values of s. Typical results are presented in Fig. 8 for $k=0.002$ in. The high tunnel noise enhances the effect of the trip for $5\times10^5<R_{\infty,D}<6.5\times10^5$. Upstream of the trip or with no trip, transition onset occurred at $R_{\infty,D}\simeq8\times10^5$ independent of tunnel noise. This value of $(R_{\infty,D})_T$ is in reasonable agreement with Poll's[9] $(\bar{R}_*)_T$ criteria and also with the Bushnell-Huffman supersonic criteria[13] of $(R_{\infty,D})_T>8\times10^5$ (see Table 2).

To facilitate comparisons with Poll's data[9] for trip wires in low-speed flow, the local reference temperature parameters $\bar{R}_*$ and k/η_* are ploted in Fig. 9 from all the present transition onset data for the $\Lambda=45$ and 60 deg models and $D=1$ in. The faired curves in this figure are subject to considerable uncertainty due to errors ($\simeq0.0003$ in.) in the measured values of k and uncertainties in the determination of $(R_{\infty,D})_T$ from the cross plots such as those shown in Figs. 7 and 8. Nevertheless, the trends of $(\bar{R}_*)_T$ with $(k/\eta_*)_T$ are similar to those of Poll[9] with respect to the effects of "critical" roughness heights. These critical roughness heights correspond to the values of k/η_* where the transition Reynolds numbers are first reduced significantly as k/η^* is increased. Thus, for $\Lambda=45$ deg, the critical values are $k/\eta_*\simeq1.4$ and 1.6 for high and low noise, respectively. For $\Lambda=60$ deg, the critical values are $k/\eta_*\simeq0.85$ and 0.95 for high and low noise, respectively. These latter values may be compared with Poll's critical values for $\Lambda\simeq60$ deg of $d/\eta\simeq0.6$ to 0.8. Poll's subcritical values of $\bar{R}_T$ were approximately 650–750, depending on the distance from the trip. It

is apparent that the present subcritical values of $(\bar{R}_*)_T$ for both sweep angles and the critical k/η_* values for $\Lambda=60$ deg agree reasonably well with Poll's values for $\Lambda \simeq 60$ deg. It is therefore concluded that the local $\bar{R}_*$ Reynolds number and k/η_* are useful correlation parameters for a wide range of freestream Mach numbers. Poll's asymptotic values of $\bar{R}_T$ for large trip wire diameters were observed for $d/\eta > 2$ and vary from $\bar{R}_T \simeq 150$–250, which are smaller than the present values from Fig. 9 for $k/\eta_* \simeq 1.7$. Obviously, larger values of k will have to be tested to determine asymptotic values for the present conditions.

Figure 9 shows that when trips are present with $k/\eta_* > 1$ for $\Lambda=60$ deg and $k/\eta_* > 1.5$ for $\Lambda=45$ deg, transition Reynolds numbers are always larger for the low tunnel noise levels than for the high noise levels. It is also concluded from Figs. 6–8 that when no trips or upstream disturbances are present, the wind-tunnel noise has no effect on transition Reynolds numbers. Both phenomena appear to agree qualitatively with trends deduced from recent stability theory on the receptivity of supersonic laminar boundary layers to acoustic disturbances in the freestream. Gaponov,[17] for example, showed that in boundary-layer flows with slow streamwise variations in the profiles or thicknesses, the external acoustic waves have the effect of generating Tollmien-Schlichting (TS) waves with excited amplitude inversely proportional to the difference in wave numbers between the acoustic and TS waves. Since the radiated wind tunnel noise is broadband, some of this noise has wave numbers that match the TS waves (see Ref. 6). Therefore, for the boundary layer on a cone or flat plate, the wind-tunnel noise has large effects on transition due to the slowly growing boundary layer. However, on a swept cylinder downstream of any end effects and with no local trip disturbances, the boundary-layer thickeness and profiles are invariant in the streamwise direction and, according to the receptivity theory,[17] there is then no mechanism for the external noise to modify the TS waves. When a trip disturbs the boundary layer locally, the external tunnel noise apparently interacts directly with TS waves along the attachment line and increases their amplitude, which in turn causes transition at lower Reynolds numbers. The relevant theoretical analysis for the linear stability of TS waves in low-speed attachment line flow has been given recently by Hall et al.[18]

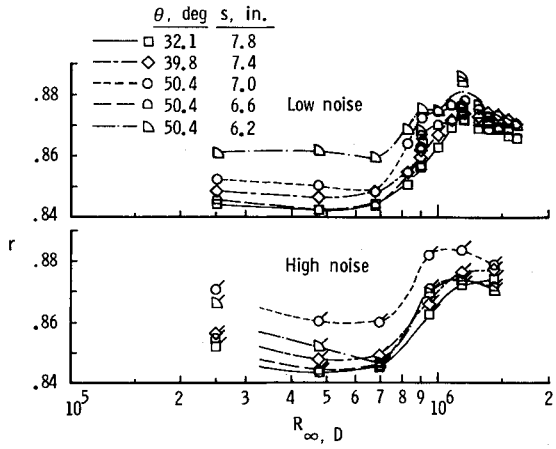

Fig. 10 Variations of r with $R_{\infty,D}$ at thermocouple locations off the attachment line. $\Lambda=60$ deg, $D=1$ in., no trips and no end plates. Flagged symbols are for the high noise condition.

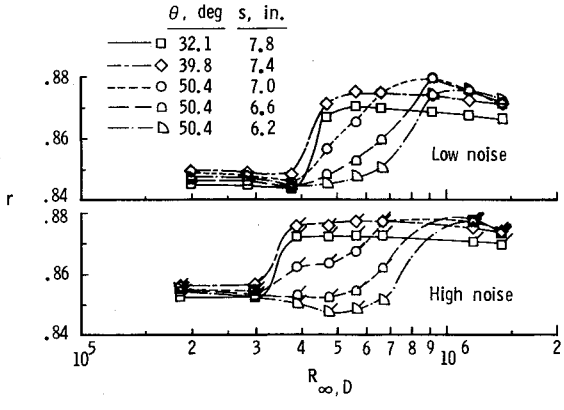

Fig. 11 Effects of noise and a trip ($k \simeq 0.004$ in. on attachment line at $s=6$ in.) on transition at locations off the attachment line. $\Lambda=60$ deg, $D=1$ in. Flagged symbols are for high noise.

Transition Downstream of Attachment Lines

The attachment line results shown in Fig. 6 also included five additional data points at each $R_{\infty,D}$ for various values of θ downstream of the attachment line. These values of r (identified as solid symbols in the figure) were obtained from temperature measurements off the attachment line (available only on the $D=1$ in. models) and the corresponding local values of T_e/T_s calculated for swept infinite cylinders from Eqs. (3) and (4). The measured s and θ locations are given in Table 3.

To show trends in transition behavior, cross plots of r against $R_{\infty,D}$ for these locations are presented in Figs. 10 and 11. Figure 10 is a cross plot for the $\Lambda=60$ deg model with no trips and no end plates for the low and high tunnel noise conditions (flagged symbols). Transition appears to occur at $R_{\infty,D} \simeq 7\times10^5$ for all five values of s and θ independent of the tunnel noise levels. It is therefore concluded again (as for the attachment line results, Fig. 5b) that with no end plate or local trip disturbances, transition up to $\theta \simeq 50$ deg is not affected by tunnel noise. The mechanism responsible for transition off the attachment line is probably the crossflow vortices. If so, these results imply that the amplification of this type of instability is not affected by the external acoustic disturbances in supersonic wind tunnels.

Figure 11 shows r plotted against $R_{\infty,D}$ for the $\Lambda=60$ deg model with a trip fixed to the attachment line at $s=6$ in. These data points are from the same runs used in Fig. 7 for which the trip height was $k=0.004$ in. The flagged symbols are for the high noise condition. For the two locations of $\theta=32.1$ and 39.8 deg with $s=7.8$ and 7.4 in., respectively, the tunnel noise again appears to enhance the trip effect and reduces $(R_{\infty,D})_T$ from about 4×10^5 for low tunnel noise to about 3×10^5 for high noise. These transition Reynolds numbers are about the same as noted previously on the attachment line (Fig. 7). For the three $\theta=50.4$ deg points, this effect of tunnel noise appears to decrease as s decreases from 7.0 to 6.2 in.; that is, as s approaches the trip location of $s=6$ in. Clearly, the point at $s=6.2$ in. is not affected by the trip because it is outside the downstream range of influence of the trip as can be determined from the general streamline orientations in the oil flow photographs of Fig. 4. Thus, it may be tentatively concluded from these few results that tunnel noise also interacts with trip disturbances off the attachment lines to further decrease transition Reynolds numbers.

Conclusions

Transition Reynolds numbers were obtained from measured recovery temperatures on swept circular cylinders at sweep angles of 45 and 60 deg. The experiments were conducted in the Mach 3.5 Pilot Quiet Tunnel at NASA Langley. The freestream noise levels were varied from extremely low values approximating those in atmospheric flight to much higher values approaching those in conventional supersonic tunnels. Data were obtained with and without trips and end plates over the freestream unit Reynolds number range from about 1.0×10^5/in. to 1.7×10^6/in. The

following conclusions are based on the results presented herein and comparisons with previous investigations.

1) Based on measured variations along the attachment lines of recovery temperatures, quasi-swept inifinite cylinder conditions were realized at about 5 diameters from the upstream ends for all end configurations tested.

2) Oil flow studies provided evidence of crossflow vortices downstream of the attachment line for laminar boundary-layer flows. Vortex wavelengths from compressible linear stability theory were in excellent agreement with the measured values.

3) End plates or large trips near the upstream ends of the models caused turbulent flow over the test Reynolds number range.

4) When all end plate and trip disturbances were removed, transition on the attachment lines occurred at freestream Reynolds numbers based on a diameter of about $7\text{–}8 \times 10^5$ in good agreement with previous correlations. These values were the same for both high and low tunnel noise.

5) The installation of small trips on the attachment lines caused transition at lower Reynolds numbers. These values were reduced still further by high tunnel noise.

6) Both of these new results concerning the effects of wind-tunnel noise on swept leading-edge transition agree qualitatively with trends deduced from Gaponov's theory on the receptivity of supersonic laminar boundary layers to external acoustic disturbances.

7) With no trip or end plate disturbances, transition off the attachment lines was also not affected by tunnel noise and occurred at about the same Reynolds numbers as on the attachment lines.

8) When the off-attachment line locations were within the downstream wedge of influence of a trip, the tunnel noise enhanced the trip effect on transition just as in the attachment line data. Transition again occurred at about the same Reynolds numbers as on the attachment lines.

References

[1]Pfenninger, W., "Flow Phenomena at the Leading Edge of Swept Wings," *Recent Developments in Boundary Layer Research—Part IV*, AGARDograph 97, May 1965.

[2]Pfenninger, W., "Laminar Flow Control-Laminarization," *Special Course on Concepts for Drag Reduction*, AGARD-R-654, March 1977, pp. 3-1—3-75.

[3]Gaster, M., "On the Flow Along Swept Leading Edges," *The Aeronautical Quarterly*, Vol. XVIII, Pt. 2, May 1967, pp. 165–184.

[4]Gray, W. E., "The Nature of the Boundary-Layer Flow at the Nose of a Swept Wing," RAE TM Aero 256, 1952.

[5]Poll, D. I. A., "Leading Edge Transition on Swept Wings," AGARD-CP-224, 1977, pp. 21-1—21-11.

[6]Beckwith, I. E., Creel, T. R. Jr., Chen, F. J., and Kendall, J. M., "Free-Stream Noise and Transition Measurements on a Cone in a Mach 3.5 Pilot Low-Disturbance Tunnel," NASA TP 2180, Sept. 1983.

[7]Gregory, N., Stuart, J. T., and Walker, W. S., "On the Stability of Three-Dimensional Boundary Layers with Application to the Flow Due to a Rotating Disk," *Philosophical Transactions of the Royal Society of London*, Ser. A, Vol. 248, 1955, pp. 155–199.

[8]Poll, D. I. A., "Three-Dimensional Boundary Layer Transition via the Mechanisms of 'Attachment Line Contamination' and Cross Flow Instability," *Proceedings of the IUTAM Symposium on Laminar-Turbulent Transition*, Springer-Verlag, Stuttgart, FRG, Sept. 1979, pp. 253–262.

[9]Poll, D. I. A., "Transition Description and Prediction in Three-Dimensional Flows," AGARD-R-709, June 1984.

[10]Poll, D. I. A., "Some Observations of the Transition Process on the Windward Face of a Long Yawed Cylinder," *Journal of Fluid Mechanics*, Vol. 150, Jan. 1985, pp. 392–356.

[11]Owen, P. R. and Randall, D. G., "Boundary Layer Transition on a Sweptback Wing: A Further Investigation," RAE TM Aero 277, 1952.

[12]Poll, D. I. A., "The Development of Intermittent Turbulence on the Swept Attachment Line Including the Effects of Compressibility," *The Aeronautical Quarterly*, Vol. 34, Feb. 1983, pp. 1–23.

[13]Bushnell, D. M. and Huffman, J. K., "Investigation of Heat Transfer to a Leading Edge of a 76° Swept Fin With and Without Chordwise Slots and Correlations of Swept-Leading-Edge Transition Data for Mach 2 to 8," NASA TMX-1475, Dec. 1967.

[14]Beckwith, I. E. and Gallagher, J. J., "Local Heat Transfer and Recovery Temperatures on a Yawed Cylinder at a Mach Number of 4.15 and High Reynolds Numbers," NASA TR R-104, 1961 (supersedes NASA MEMO 2-27-59L).

[15]Reshotko, E. and Beckwith, I. E., "Compressible Laminar Boundary Layer Over a Yawed Infinite Cylinder With Heat Transfer and Arbitrary Prandtl Number," NACA TR-1379, 1958.

[16]Beckwith, I. E., "Similar Solutions for the Compressible Boundary Layer on a Yawed Cylinder with Transpiration Cooling," NASA TR R-42, 1959 (supersedes NACA TN 4345).

[17]Gaponov, S. A., *Excitation by Sound of Tollmien-Schlichting Waves in a Supersonic Boundary Layer*, Plenum Publishing Corp., New York, 1983 (translated from *Izvestiya Akademiii nuk SSSR, Mekhanika Zhidkosti i Gaza*, No. 3, May-June 1983, pp. 59–66.

[18]Hall, P., Malik, M. R., and Poll, D. I. A., "On the Stability of an Infinite Swept Attachment Line Boundary Layer," *Proceedings of Royal Society of London*, Ser. A, Vol. 395, 1984, pp. 229–245.